



Effect of layer-by-layer synthesized graphene–polyaniline-based nanocontainers for corrosion protection of mild steel

Siddhant Varshney¹, Karan Chugh¹, and S. T. Mhaske^{1,*}

¹Department of Polymer and Surface Engineering, Institute of Chemical Technology, Nathalal Parekh Marg, Matunga (E), Mumbai 400019, India

Received: 4 December 2021

Accepted: 6 April 2022

Published online:

20 April 2022

© The Author(s), under exclusive licence to Springer Science+Business Media, LLC, part of Springer Nature 2022

ABSTRACT

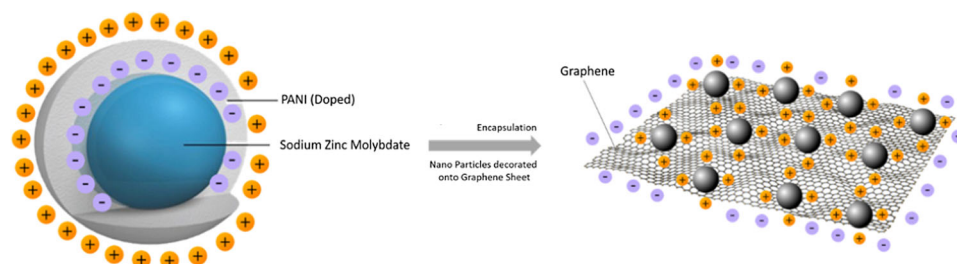
Graphene and polyaniline have been shown to have superior anti-corrosive properties due to barrier formation. As single-layer graphene is porous and, due to percolation, can also encourage corrosion; hence, an attempt has been made to cover the graphene layers with doped conducting polyaniline to further enhance anti-corrosion. Sodium zinc molybdate nanoparticle is used as the core material to get entrapped into graphene–polyaniline-based nanocontainer to achieve superior anti-corrosive property. Inexpensive methods are used to synthesize all materials to make this process as economic as possible. Nanocontainer synthesis has been done by a layer-by-layer technique. Few layered graphene sheets and polyaniline nanofibres have been successfully incorporated to entrap sodium zinc molybdate nanoparticles (280 nm) and tested for anti-corrosion application in epoxy-based systems for MS (mild steel) panels. Scanning electron microscopy (SEM) and transmission electron Microscopy (TEM) images show flower-like morphology of sodium zinc molybdate nanoparticles, which have been synthesized by a novel method. Various characterisations like zeta potential, particle size, Fourier transform infrared spectroscopy (FTIR), and thermogravimetric analysis (TGA) suggest the successful formation of nanocontainers, and EIS plots suggest good anti-corrosive behaviour of the resultant coatings.

Handling Editor: Maude Jimenez.

Address correspondence to E-mail: st.mhaske@ictmumbai.edu.in
E-mail Addresses: siddhant.varshney@yahoo.in; karan.chugh94@gmail.com

GRAPHICAL ABSTRACT

NZM-PANI decorated graphene sheets



Introduction

Corrosion is a natural process by which metals attain their thermodynamically stable oxide form. Metals are almost useless to the industry in this steady state and can only be utilized to their full potential by reducing it to the pure metallic form. To control corrosion, cathodic and anodic protection may be used depending on the corrosive environment and corroding species. Zinc galvanization is an example of cathodic protection. Barriers can also help protect the substrate by blocking any ions responsible for corrosion, e.g. water molecules, salt ions, acid ions, and oxygen. Organic coatings are an excellent example of one such barrier layer that provides excellent adhesion to the substrate and controlled porosity for the protection of substrate for several years. Many organic coatings have been used in the past, like polystyrene, epoxy, PU, alkyds, acrylics in their pure form, and dispersed specialized nanoparticles. Specialized nanoparticle functionalized/ designed so that it helps protect the surface of the substrate by providing a passivating effect or releasing corrosion inhibitors that provide sacrificial cathodic protection [1]–[10].

The synthesis of cross-linked polyaniline (PANI) by a novel solvothermal metathesis reaction of *p*-dichlorobenzene ($C_6H_4Cl_2$) with sodium amide ($NaNH_2$) in benzene at 220 °C [11]. Sonochemical synthesis of polyaniline nanofibres, micro-sized irregular polyaniline (PANI) particles synthesized by

dropwise addition of the ammonium persulfate (APS) solution into the aniline (ANI) solution with mechanical stirring. PANI nanofibres in diameters of ~ 50 nm (nm) and lengths of 200 nm to several micrometres are prepared [10, 12]. Polyaniline-*y*-aminopropyltriethoxysilane-titania nanotube arrays (PANI-APTES- TiO_2 NTA) nanocomposite through a graft polymerization of PANI on the surface of the self-assembled monolayer (SAM) coated TiO_2 NTA after anodized TiO_2 NTA was modified by APTES [13]. Anti-corrosive properties of PANI by dispersing inorganic (hydrochloric, phosphoric, and sulfuric) and organic (*p*-toluenesulfonic and 5-sulfosalicylic) acid-doped PANI salts into alkyd, with different PVC (1,5,10,15%) [14]. The process to produce single sheets of functionalized graphene through thermal exfoliation of graphite oxide. The process yielded a wrinkled sheet structure resulting from reaction sites involved in oxidation and reduction processes [15]. Graphene/polyaniline nanocomposite by the in situ oxidative polymerization of aniline in the presence of graphene and the surfactant, cetyl trimethyl ammonium bromide (CTAB). The micellar structure of CTAB assisted both the formation of graphene/polyaniline tubules and the dispersion of graphene [4]. The composite of polyaniline and reduced graphene oxide (PANI/RGO) was prepared through polymerization of aniline in graphene oxide and further reduction by hydrate hydrazine. It was an effective adsorbent towards mercury(II) adsorption in aqueous solutions [2, 13].

Synthesis of exfoliated graphite materials which were rapidly and efficiently prepared by microwave irradiation in a short time (about 4 min including 3 min mixing and 1 min microwave irradiation). The promotion of intercalation by microwave irradiation was proven by X-ray diffraction [16–19]. An improved method to synthesise graphene oxide, different from the popular Hummer's method, where explosive chances are reduced to almost zero. They excluded NaNO_3 increased the amount of KMnO_4 and used it as a 9:1 mixture of $\text{H}_2\text{SO}_4/\text{H}_3\text{PO}_4$ to show an increased efficiency in oxidation. Moreover, toxic gas was not generated, and temperature could be easily controlled [20, 21].

Zinc molybdate rod-like nanostructures had been successfully synthesized by precipitation method process and using a solid organometallic molecular precursor [bis(salicylaldehyde)zinc(II)], $\text{Zn}(\text{sal})_2$, and $(\text{NH}_4)_6\text{Mo}_7\text{O}_{24}\cdot 4\text{H}_2\text{O}$ as starting materials [7, 22]. Approach to synthesize sodium zinc molybdatenano-pigment using ultrasound-assisted co-precipitation of sodium molybdate and zinc oxide. X-ray diffraction, Fourier transform infrared and elemental analysis of sodium zinc molybdatenano-pigment had been performed, which confirmed the formation of sodium zinc molybdate particles. Ultrasound-assisted synthesis gave smaller particle sizes of sodium zinc molybdate nanoparticles (467 nm) which could be explained based on improved solute transfer rate, rapid nucleation, and formation of a large number of nuclei in the presence of ultrasound. The corrosion inhibition effect of sodium zinc molybdatenano-pigment in 2 K (two-pack) epoxy-clear polyamide coat on low carbon steel was also studied. The results of the corrosion rate analysis, Tafel plots, and electrochemical impedance spectroscopy of the prepared coatings showed better corrosion inhibition performance when sodium zinc molybdate particles were incorporated in the 2 K epoxy-polyamide clear coat [6, 23]–[25]. Encapsulating a corrosion inhibitor like benzotriazole drastically improves corrosion protection as the corrosion inhibitor forms a protective layer on reaction with the metal substrate and prevents further corrosion. Apart from using a corrosion inhibitor, materials like chromium, molybdate, zinc, magnesium, and sodium provide corrosion protection by forming insoluble precipitates with hydroxyl or chloride ions, forming a passivating layer. This research has used no corrosion inhibitor due to its high toxicity. Sodium zinc molybdate nanoparticles

have been encapsulated by doped polyaniline, which is then decorated onto graphene sheets by two approaches, namely layer by layer and covalent bonding. The three moieties have been selected due to their excellent anti-corrosion properties [26]–[30].

The present work aimed to develop nanocontainers that can be dispersed into a paint system (epoxy) to enhance its anti-corrosive performance. The project's central theme is graphene–polyaniline-based nanocontainer with sodium zinc molybdate as a core material. This core–shell arrangement is being made by the layer-by-layer method. Magnesium zinc molybdate has been shown to exhibit barrier properties against corrosion [31] which is comparable to the performance of sodium zinc molybdate. Graphene has been used as a protective barrier against corrosion [32]. Polyaniline also has been shown to exhibit high anti-corrosive properties [33, 34]. Hence, all three components are individually capable of protecting metal from corrosion.

Materials and methods

Materials

Hydrochloric acid (HCL), acetone, graphite, nitric acid, sodium molybdate, aniline, zinc oxide, sulfuric acid (H_2SO_4), orthophosphoric acid, and hydrogen peroxide (H_2O_2) were procured from S. D. Fine Chemicals Ltd., Mumbai, India. Ammonium persulfate (APS) was received from Thermo Fischer scientific India Pvt Ltd., Mumbai, India. Epoxy resin (low viscosity 530–690 MPa) was received from Champion advance materials private limited, Mumbai, India. Polyether amine (Jeffamine) was received from BASF, Mumbai, India and Potassium permanganate was received from Pallav Chemicals, Mumbai, India.

Synthesis of sodium zinc molybdate (NZM)

Zinc oxide powder (0.489 g in 15 ml, 0.4 M) was added to a round bottom flask. A sufficient amount of nitric acid (just about to dissolve the zinc oxide powder) is added and heated to remove excess acid. The solution is stirred until all the ZnO is dissolved. Then, sodium molybdatedihydrate (2.904 g in 15 ml, 0.8 M) was added to the solution and was stirred thoroughly. Then, the reactor was set up in the heater-stirrer apparatus and stirred for 1 h at 1500 RPM

at 80°C (With condenser and all other necks closed). After that, it was let to stir for about half to one hour at the same temperature at a higher RPM of 1800. (An increase in time of stirring leads to the decreased size of nanoparticles). It was observed that white precipitate was generated in about 45 min of stirring. The precipitate was then centrifuged for 20 min at 2000 RPM. The filtered product obtained after decantation was then dried for 0.5 h at 80 °C. (Tables 1, 2, 3, 4, 5, 6).

Synthesis of polyaniline (PANI)

APS:Aniline molar ratio is fixed at 1.25:1, after attempting various ratios of 0.5:1 to 1.5:1. APS is dissolved in 100 mL of 1M aqueous acid solution. This solution is then added to undiluted aniline and sonicated for 2 h at a temperature below 25 °C. Rapid addition is followed here [35] to get the best results for anti-corrosive properties and achieve small particle size, contrary to the conventional method where dilute aniline is added dropwise to the APS solution. This method also saves reaction time.

Synthesis of graphene

Liquid exfoliation of graphite using acetone and water

Figure 1 shows the synthesis of graphene from graphite, acetone (83.35 ml) and water (16.65 ml) were mixed thoroughly, and graphite (0.3 g) was added to the mixture. The mixture was sonicated for 4 h in a bath sonicator in an enclosed glass vessel with a temperature ranging between 20 and 25 °C. The resulting dispersion was centrifuged for 30 min at 2500 RPM. [36] The centrifuged dispersion was then kept for drying in an air oven for 2 h at 80°C. Graphene sheets, at around 114 g, are optimized to give the best dispersed and highly exfoliated with the least body defects.

Calculation for g force:

$$g = \{1.118 \times 10^{-5}\} \times r \times r \times (\text{rpm}^2).$$

r = radius of centrifugation machine.

rpm = revolutions per minute.

SDS treatment of sodium zinc molybdate

Sodium zinc molybdate (NZM) nanoparticles were treated with SDS (0.01wt%). An aqueous solution of SDS is prepared in 100 ml DI water, and NZM particles are added subject to sonication for 5 min. Foaming is seen to reduce, primarily indicating the formation of the SDS layer onto NZM. This is passed through vacuum filtration onto a glass crucible (grade 5) followed by washing with DI water. This is done to remove unreacted SDS from the system. The cake is dried at 65 C for 2 h.

Formation of PANI layer onto NZM

PANI dispersion is prepared by bath sonication into 100 mL DI water for 5 min. To this, SDS-treated NZM dispersion is added (pre-sonicated) in 10 ml DI water. The weight ratio of PANI:NZM is kept at 3:1 to achieve a net positive zeta value. The reaction is kept for 10 min under bath sonication at 40 Hz. The colour of PANI dispersion changes from dark green to light green during the process. The product is then vacuum filtered onto Grade 5 Glass crucible, followed by multiple washings with DI water. The filter cake is dried at 65°C for 2 h. If removal of cake is problematic, then one can add a slight amount of DI water to the filter cake and sonicate the glass crucible, thus forming a dispersion. This dispersion can be dried on a Petri dish at 65°C overnight, giving dried cake that can be easily peeled off. The layer-by-layer process is being followed for the formation of the shell onto the core.

Formation of graphene layer onto NZM-PANI

Graphene dispersion is prepared by sonicating graphene particles into 100 ml DI water for 5 min. After sonicating NZM-PANI particles in 10 ml DI water, it is added to graphene dispersion. Graphene: PANI:NZM wt. ratio is kept at 6:3:1 to achieve a proper coating of graphene sheets and give net zeta value negative. This system is kept for bath sonication at

Table 1 Experimental data for sodium zinc molybdate

Sodium molybdatedihydrate	Zinc oxide	DI water	Nitric acid	Reaction time	Reaction temperature	Yield
2.904 g	0.489 g	30 mL	1 mL	2 h	80 °C	98%

Table 2 Experimental data for polyaniline

Aniline	APS	Acid	Time	Temperature	Yield
1.86 g	5.7 g	1 M (100 mL solution of aqua regia)	1 h	10 °C	96–98% in all concentrations

Table 3 Experimental data for acetone–water exfoliated graphite

Acetone	Water	Graphite	Reaction temperature	Reaction time	Yield
83.35 mL	16.65 mL	0.3 g	20 °C	4 h	60%

Table 4 Experimental data for SDS treatment of sodium zinc molybdate

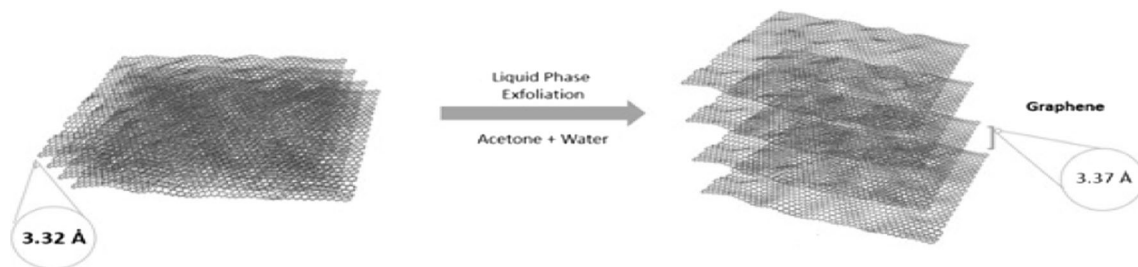
NZM	SDS	Water	Reaction Temp	Reaction Time	Yield
1 g	0.001 g	100 mL	RT	0.5 h	99%

Table 5 Experimental data for PANI encapsulation of sodium zinc molybdate

PANI	NZM-SDS	DI water	Reaction temp	Reaction time	Yield
0.1 g	0.3 g	100 mL	30 °C	2 h	99%

Table 6 Experimental data for decoration of NZM-PANI particles onto graphene sheets

Graphene	NZM-PANI	DI water	Reaction temp	Reaction time	Yield
0.6 g	0.4 g	100 mL	30 °C	2 h	99.1%

**Figure 1** Synthesis of graphene.

40 Hz for 10 min. The dark black colour of graphene dispersion changes to greyish green during the process, indicating the layer-by-layer process taking place. The solution is then vacuum filtered, giving greyish green particles. The filter cake is dried at 65 °C for 2 h.

Paint formulation

Epoxy resin was treated with a polyether amine (Jeffamine) hardener in the weight ratio 1:0.575 as per equivalent weight calculations, keeping molar stoichiometry 1:1. 1 wt% nanoparticle was dispersed in the paint for 10 min at 1000 rpm for uniform

distribution, and the paint was drop-down coated on MS steel panels.

Surface preparation of mild steels panels

ASTM G-1 standard was followed for the preparation of mild steel (MS) substrate for anti-corrosion study of PANI-Graphene/Epoxy-coated samples. MS panels having dimensions 6 X 4 inches with 1.5 mm thickness were used. Substrate for the coating was at first cleaned and polished with the help of fine emery paper of P40, P80, P220 and P400 grade, respectively. The surface was then cleaned with ethanol just before the application of the composite.

Analysis

TGA

Thermogravimetric analysis (TGA) is a technique, wherein the loss of mass of a substance is monitored as a function of temperature or time, while the sample specimen is subjected to a controlled temperature programme in a controlled atmosphere. TGA of raw sample and after each treatment was performed using Pyris 1 instrument of PerkinElmer. The tests were carried out at a temperature range from 30 to 600 °C with a heating rate of 20 °C/min under nitrogen gas. The decrease in percentage weight loss is recorded.

FTIR analysis

Fourier transform infrared spectroscopy (FTIR) is the analytical technique for monitoring functional group changes in samples. Characterization of dried samples at every step was done using an Alpha instrument from Bruker, the USA using the KBr pellet method to analyze the changes in formation and breaking of various bonds. Before preparing the pellet, KBr was kept in the oven for 1 h at 150 °C. The resolution was set at 4 cm⁻¹ with a range of 4000 cm⁻¹ to 500 cm⁻¹ with 24 scans.

PSD

Particle size measurements have been widely employed in the characterization of nanoparticles to determine the range of the particle. Particle size distribution (PSD) of various stages was determined using a NanoPlus zeta/nanoparticle analyzer instrument from Particulate Systems. The sample was sonicated before use. 5 mL of the turbid aqueous suspension was placed in a quartz cuvette after shaking, and the determination was performed. The test is carried out through DLS (Dynamic Light Scattering) where the Brownian motion of particles is studied. The larger particles tend to show slow motion, whereas smaller particles have a higher average velocity.

XRD

X-ray diffraction (XRD) is principally used to determine the crystalline structure of materials. Wide-

angle XRD patterns of samples before and after treatment were obtained using powder XRD system of Bruker D8 Advance instrument with CuK α radiation ($k = 1.54 \text{ \AA}$) for the confirmation of the diffraction patterns. The diffractometer was operated at 30 kV and 15 mA. The measurements covered the scanning range of 5°–90° at a scanning speed of 2°/min.

SEM/EDAX

Scanning electron microscopy (SEM) on a JEOL, JSM-6380 LA 15 kV electron microscope, Transmission Electron Microscopy (TEM) on Technai G20 working at 200 kV. This testing was carried out at ICON Analytics, Mumbai, India. Samples were sonicated before analysis. EDAX was carried out on the same instrument.

TEM

High-resolution transmission electron microscopy (HR-TEM) on Technai G2 working at 300 kV was done at IIT Bombay SAIF (Sophisticated Analytical Instruments facility), Mumbai, India. Graphene-based samples were placed on lacey substrates to avoid sample deterioration on exposure of electron beams. A very dilute solution of samples was placed onto a small sample holder. This was dried for 1 h under IR radiation.

Anti-corrosive tests

EIS (Linear polarisation) and salt spray tests were carried out for anti-corrosive property determination. The panels made of mild steel (150 mm \times 100 mm \times 0.5 mm) were cleaned and coated with prepared formulations. The anti-corrosive properties of coated panels were carried out in 5 wt% aqueous NaCl solution as an electrolyte at room temperature (25 °C) on Versa STAT-3 instrument. The coated plate was used as a working electrode, while Pt and saturated calomel electrode (SCE) were used as counter and reference electrodes. Bode plot test was carried out with a similar setup and frequency ranging from 0.001 to 10⁵ Hz.

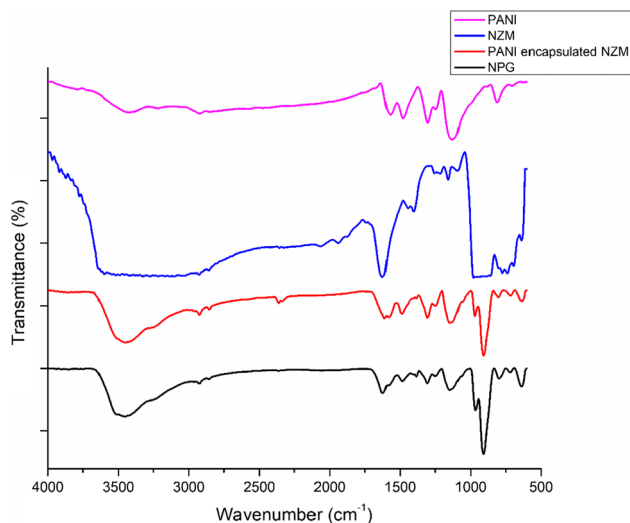


Figure 2 FTIR of sodium zinc molybdate (NZM), PANI, PANI encapsulated NZM, NPG.

Results and discussion

FTIR analysis

Figure 2 shows the Fourier-transform infrared spectroscopy (FTIR) of sodium zinc molybdate (NZM), PANI, PANI encapsulated NZM, NZM-PANI-Graphene (NPG) identified in the huge distributed range of 600–4000 cm^{-1} . The peaks between 630–775 cm^{-1} depict the overlapping bands of sodium zincate and molybdate ion. Those at 980 cm^{-1} were specified as Mo–O stretching in the bridging of Mo–O–Mo. Also, a very strong peak was observed at around 800 cm^{-1} depicting $[\text{MoO}_4]^{2-}$. The characteristic peak at 1157 cm^{-1} shows the Mo–O–H bending in NZM molecules. The vibrational spectra are also sensitive to the changes in the electronic structure of polyaniline. Absorption bands in the region 3400–2800 cm^{-1} are connected with nitrogen-containing groups, such as the secondary amine $-\text{NH}-$ and protonated imine $-\text{NH}^+ =$. They reflect the organization of polyaniline chains within the film by hydrogen bonding involving these groups.

A broad absorption band typical of the conducting form of polyaniline is observed at wavenumbers above 2000 cm^{-1} . Two main bands with maxima situated at 1569 and 1477 cm^{-1} , assigned to quinoid and benzenoid ring stretching vibrations, respectively, dominate the spectrum in the region below 2000 cm^{-1} . The absorption band situated at 1305 cm^{-1} corresponds to π -electron delocalization induced in

the polymer by protonation. The band of CN + stretching vibrations in the polaronic structure is observed at 1246 cm^{-1} . The prominent band situated at 1128 cm^{-1} –1136 cm^{-1} , which is formed during protonation, has been assigned to the vibrations of the $-\text{NH}^+ =$ structure. The region 900–700 cm^{-1} corresponding to the aromatic ring out-of-plane deformation vibrations is represented by a band located at 810 cm^{-1} , which belongs to C–H deformations in the para-substituted ring. The FTIR shows dampening of NZM peaks due to PANI encapsulation, as IR radiations are unable to penetrate through thick PANI layers (200 nm thick) efficiently. Peaks at 1485 and 1623 cm^{-1} show benzenoid and quinoid stretches, respectively, with a higher intensity quinoid stretch. The absorption band situated at 1305 cm^{-1} corresponds to π -electron delocalization induced in the polymer by protonation. Peaks at 1146 and 967 cm^{-1} show Molybdenum–O and O–Mo–O stretches characteristic of sodium zinc molybdate nanoparticles. FTIR peaks of NPG are very similar to NZM–PANI, as the number of particles attached to each graphene sheet is very high. Hence, peaks of NZM–PANI are predominant. Moreover, graphene sheets as seen by TEM images are very thin and IR rays can penetrate through them easily. Graphene also shows neutrality to IR rays to a large extent, due to the presence of only C bonds. However, the peak at 1404 cm^{-1} shows a double bond stretch of C–C. This indicates graphene grafting onto NZM–PANI nanoparticles.

XRD

The XRD patterns in Fig. 3 show a broad peak centred at about 19.54 (d spacing 4.54 Å), which is mainly ascribed to the periodicity parallel to the polymer chain. From the XRD patterns, the product is almost amorphous and the periodicity perpendicular to the polymer chain is completely missing. [35, 37] even reported that polyaniline (EB) would become completely amorphous from partially crystalline after annealing at 215 °C because of a non-reversing chemical cross-linking reaction. The strongest peaks are at 25–26 (2θ), giving average d -spacing as 3.5 Å. The crystallinity of PANI is 17.36%.

Figure 4 shows the XRD patterns of the NZM compound prepared sonochemically at 80 °C. The diffraction peaks at 2θ value of 25.2, 27.2, 29.1, 31.7, 34.3, 47.6 and 52.8 correspond to the planes (112), (002), (114), (211), (200), (220) and (312) are assigned

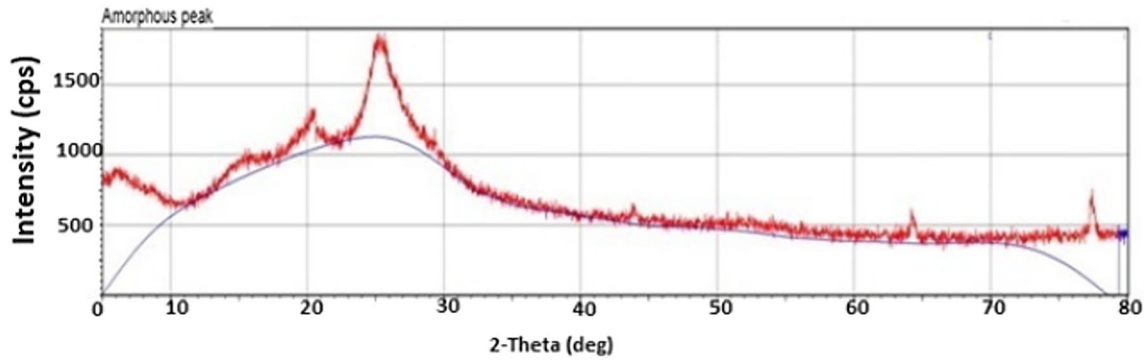


Figure 3 XRD of PANI nanofibres.

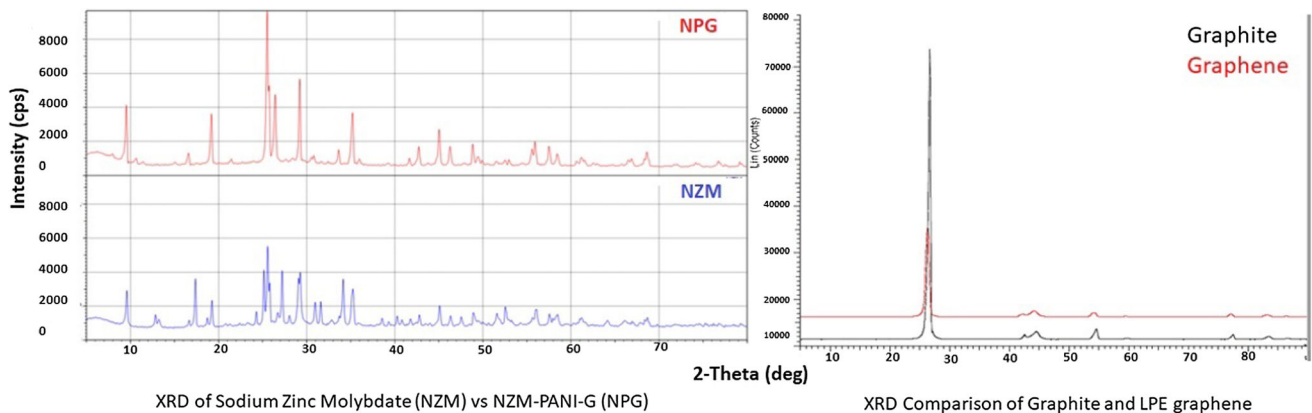


Figure 4 XRD of sodium zinc molybdate (NZM), NZM-PANI-Graphene (NPG), graphite and graphene.

to the sodium zinc molybdate compound. The position of the peaks denotes the presence of sodium molybdenum oxide (33–0330) and zinc molybdate (25–1024), i.e. sodium zinc molybdate. The presence of these peaks confirms the formation of NZM compounds [38]. It is also found that the formed NZM nanoparticles are crystalline. The diffraction pattern of NZM prepared by the conventional method at 80 °C shows less intense peaks confirming the formation of less crystalline NZM by the conventional method. Whereas in the case of sonochemically prepared NZM compound at 80 °C temperature diffraction peaks show improved intensity, indicating an enhancement in the crystallinity due to the suitable environment created by ultrasonic irradiation. The strongest peaks occur in the 2θ range of 25°–30°, indicating an average d -spacing of 3.5 Å. The crystallinity of the NZM is 30%. The peak of graphene is at 26.43° (2θ), and d spacing of 3.367 Å. The peak of graphite is at 26.72° (2θ), and d spacing of 3.331 Å. Hence, total exfoliation is about 0.0355 Å. Hence,

liquid-phase exfoliation (LPE) was able to exfoliate the graphite sheets successfully. Other minor peaks are due to defects in the graphite structure. The peak intensity in graphene treatment has increased in intensity as well as sharpness, as crystallinity increases with graphene incorporation. However, it can be seen clearly that the major contributor to XRD patterns is the core particle, sodium zinc molybdate. The crystallinity of NPG is about 34.13%, which is 4.2% higher than that of original sodium zinc molybdate nanoparticles. This can be attributed to large amounts of graphene sheets present in the system. The strongest peaks are at 2θ ranges 25.49°, 29.18°, 25.72° giving an average d spacing of 3.5 Å which is very close to the d spacing value for the original sodium zinc molybdate. This indicated that due to the crystallinity of NZM being high, it had a major contribution to the XRD behaviour of the final product. Comparative presentation for NZM and NPG can be seen in Fig. 4.

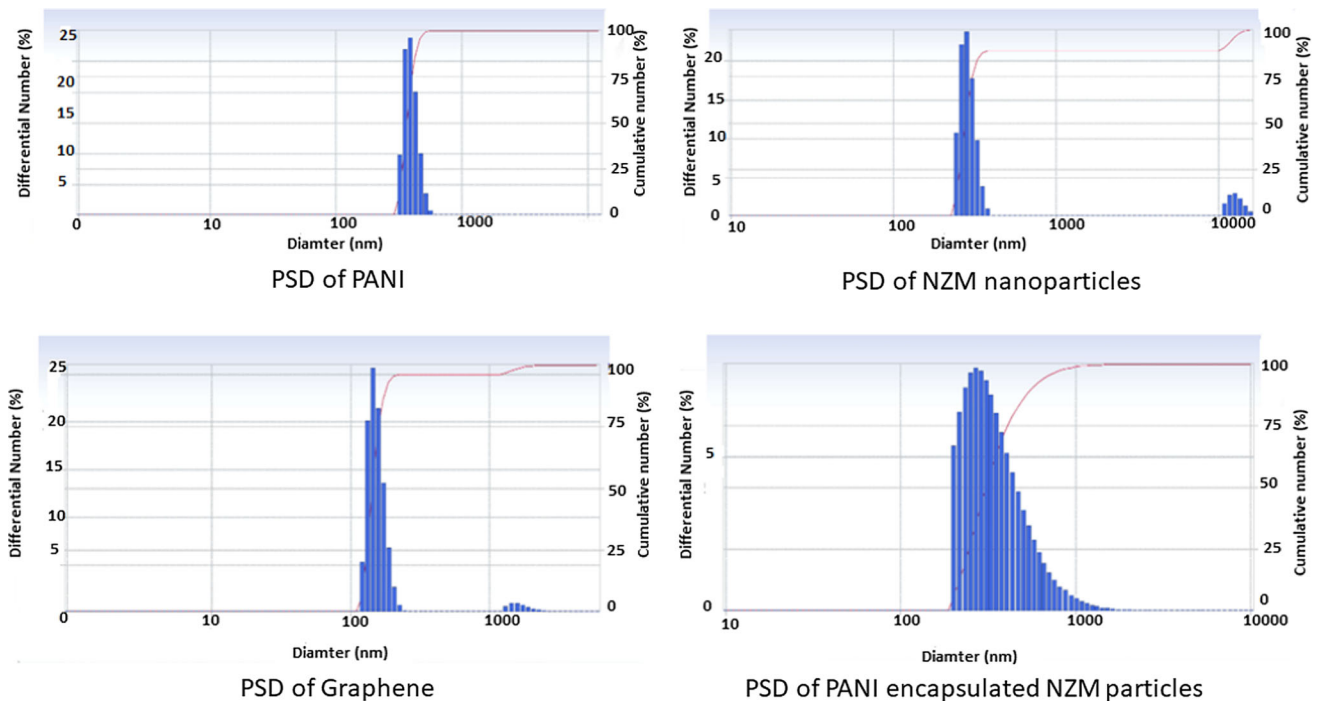


Figure 5 PSD of PANI, NZM nanoparticles, graphene dispersion (Number distribution) and PANI encapsulated NZM particles (Volume Distribution).

Particle size

Figure 5 indicates the particle size distribution of NZM and PANI shows 88.8% of particles in the range of 244.5–384.2 nm. Number distribution study was carried out after 2 h of synthesis; hence, some amount of agglomeration can be seen beyond the 10,000 nm size range. The refractive index of dispersion was 1.33 and the standard deviation of 30.3. The test was carried out at ambient room temperature and after SDS treatment. The cumulant diameter is 346.2 nm, which does not include the sheet thickness. The thickness of graphene sheets is far less compared to their width. 90% of the particles lie in the range of 150–180 nm, with a standard deviation of 21.4. As shown in the figure, PANI encapsulated NZM particles show a cumulant diameter of 643.9 nm and 90% of particles lie within the 576 nm range, with a standard deviation of 186.1. PANI encapsulation shows an increase of 200 nm size, indicating a thick coating of PANI, as its weight ratio was kept at 3:1 for NZM.

Zeta potential

In Fig. 6, the zeta potential of SDS-treated NZM nanoparticles was found to be -33.15 mV. The negative charge arises due to the anionic behaviour of SDS surfactants. It can be noted that an addition of a very small amount of SDS can bring about a large change in zeta potential. Mixing of NZM and PANI in a 1:3 wt ratio, PANI is seen to change the polarity of the charge on the particle surface (9.07 mV), making it able to further allow graphene sheets to be decorated onto it. The negative charge on graphene sheets, due to which zeta potential was found to be -24.94, is because of pi-electron clouds present in the backbone structure. Due to their conjugation, the pi-electron cloud can move freely throughout the chain. Also, mobility in the order of 10^{-4} can be attributed to the ultrathin size of graphene sheets, making events like quantum tunnelling happen more frequently. Quantum tunnelling increases electron mobility significantly. PANI and graphene were mixed in a 1:1 wt ratio in an aqueous medium to obtain PANI-decorated graphene sheets. PANI nanofibres were able to get the surface charge of graphene to change its polarity, obtaining an overall zeta potential of +14.47 mV (Fig. 7). It can be observed that equal

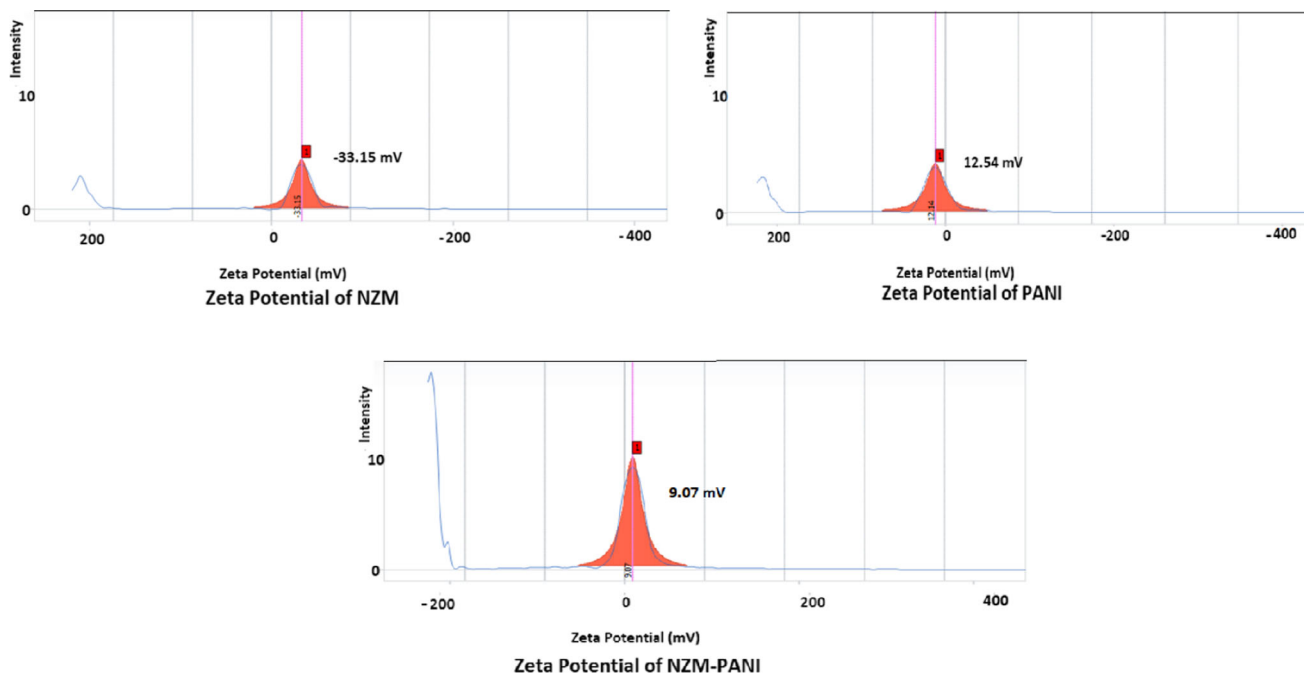


Figure 6 Zeta potential of NZM nanoparticles, PANI, NZM-PANI.

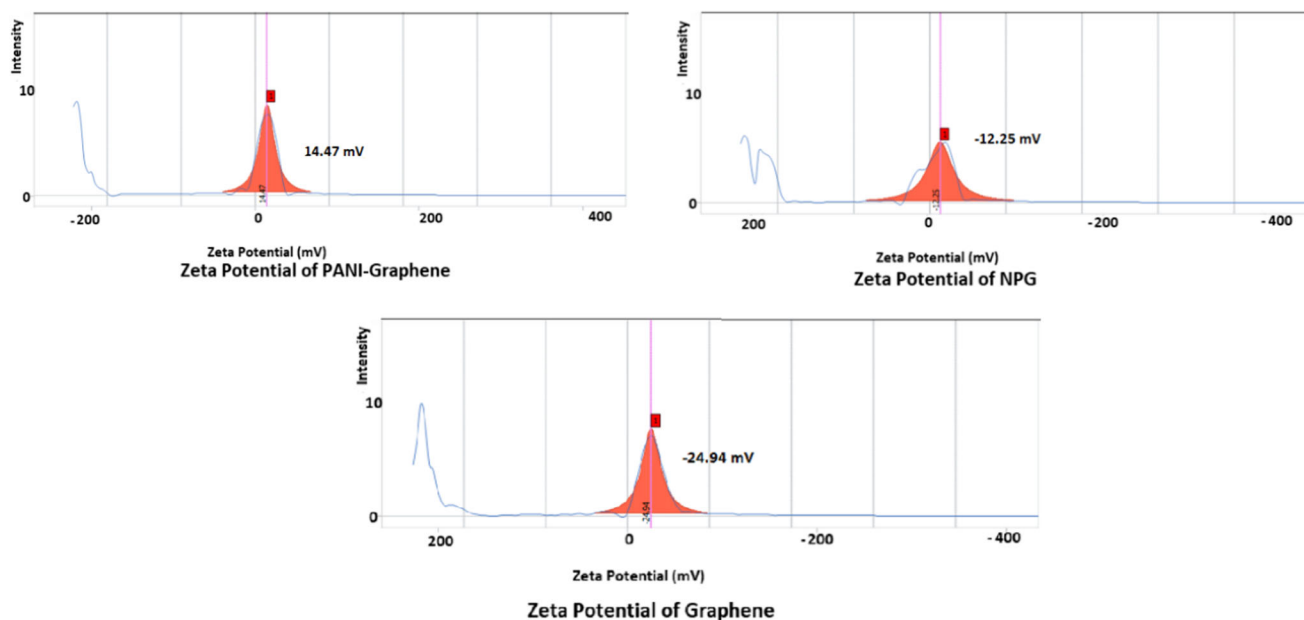


Figure 7 Zeta potential of PANI-Graphene, NZM-PANI nanoparticles decorated onto graphene sheets, graphene.

weight PANI is enough to change the polarity of the charge on graphene, but not on NZM. Hence, it can be assumed that decorating efficiency of PANI onto graphene is much more than its encapsulation efficiency onto sodium zinc molybdate (NZM). The overall zeta potential of PANI encapsulated NZM particles could come down to -12.25 mV from $+$

9.07 mV (NZM-PANI) when graphene was incorporated, showing a successful decoration onto graphene sheets.

SEM

Figure 8 indicates the SEM of sodium zinc molybdate and PANI nanofibres, with a reactivity ratio of 1:1,

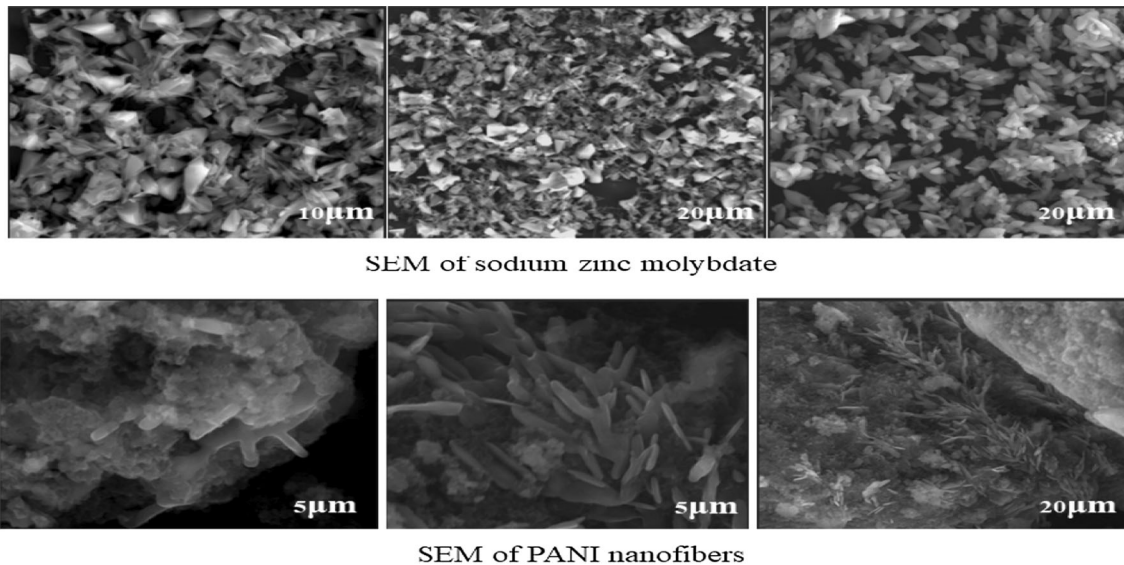


Figure 8 SEM of sodium zinc molybdate and PANI nanofibres.

some quantity of sodium is lost to excess nitric acid as sodium nitrate, hence decreasing the yield of sodium zinc molybdate. Here, crystal-like structures of zinc molybdate are predominant as sodium is unable to fully get utilised in the reaction. However, very little agglomeration can be seen owing to zeta potential development on the surfaces thus indicating a high surface area for further reaction. These particles are also proven to give excellent anti-corrosion properties in other studies [31]. With the addition of excess sodium molybdate, sodium was able to get fully utilised and form a high yield of sodium zinc molybdate. However, this product acts as a nucleating agent for excess molybdate ions to crystallise into a flower-like structure. This phenomenon is generally shown by molybdate-containing compounds and is being thoroughly studied [38]. Slight shine on a few particles indicates storage of charge hence indicating capacitive behaviour of such nucleated flower-like particles to some extent. Petals of this flower-like structure are sensitive to electrons; therefore, few broken petals can also be seen in the image, which becomes more prominent during TEM analysis. At magnifications of 5000x, it becomes clear that there is a nanofibre formation of polyaniline, and fibres have a diameter of about 50 nm. There are a few cotton-like structures also seen in the image, which indicate agglomeration as the sample had been tested after 2 days of synthesis. Agglomeration rate is observed to be fast in the case of polyanilines synthesised by oxidative polymerisation. If SEM of PANI is taken as

soon as it is synthesised, only nanofibres can be seen [39]. Agglomeration becomes prominent within 4 h of synthesis. However, agglomeration only has a marginal effect on anti-corrosive properties, making it an acceptable feature. The shine present in the image with 5000 × magnification indicates the capacitive behaviour of polyaniline.

At a magnification of 4000 × and 2000 ×, graphene sheets can be observed. Transparency indicates the presence of few-layered and single-layered structures, showing successful exfoliation of graphite sheets. As can be seen, the surface area of graphene sheets is quite large compared to the particle size of sodium zinc molybdate as well as polyaniline-graphene composites. Due to its size, it is extremely tough to wrap graphene sheets onto such small-sized particles; hence, thermodynamics favours the formation of nanoparticle-decorated graphene sheets, which becomes clear in TEM analysis.

In Fig. 9, at a magnification of 5000 × and 10,000x, it can be seen that positively charged PANI nanofibres have covered the surface of negatively charged NZM and aggregations are seen in some places due to agglomerating tendency of PANI. PANI weight ratio with respect to NZM is 3; hence, more amount of PANI nanofibres per unit area can be seen. We can see that the particle size of individual NZM particles has reduced due to higher interlayer separation because of PANI encapsulation.

In Fig. 10, negatively charged graphene sheets are seen to cover PANI encapsulated NZM particles

Figure 9 SEM of liquid-phase exfoliated graphene sheets and PANI encapsulated NZM nanoparticles.

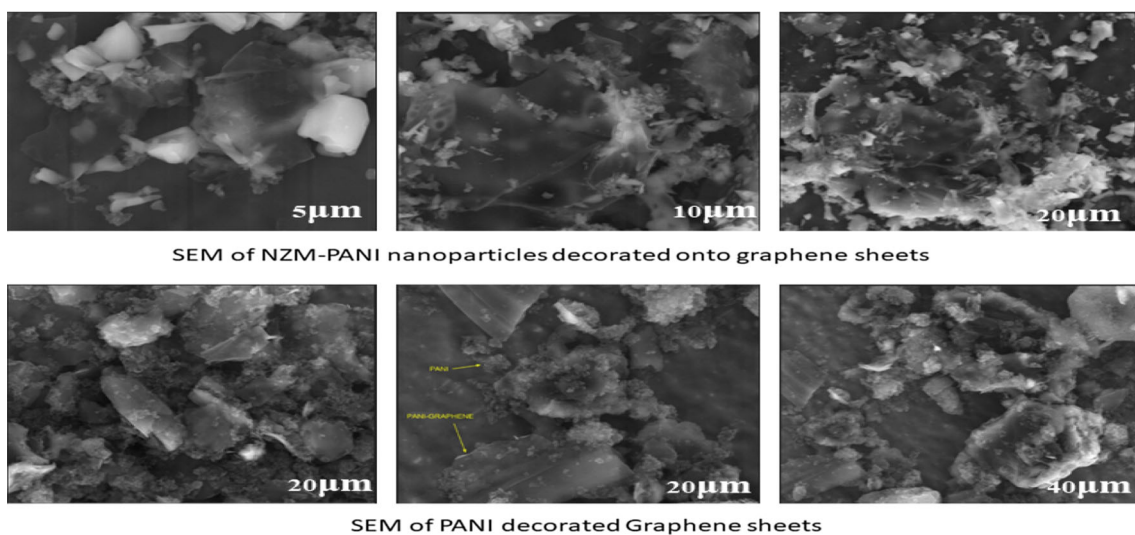
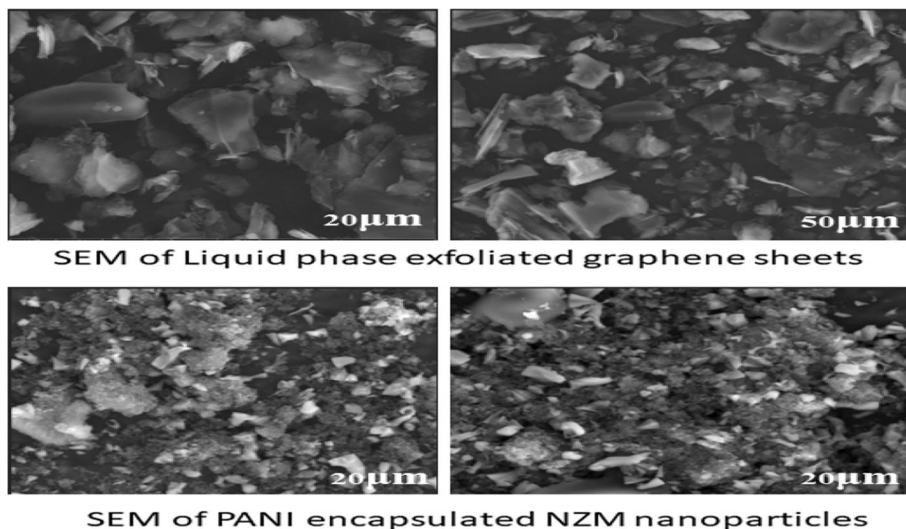


Figure 10 SEM of NZM-PANI nanoparticles decorated onto graphene sheets and PANI decorated graphene sheets.

successfully. At a magnification of $10,000\times$ and $20,000\times$, the graphene layers, due to their transparency, can be said to be few-layered and seem to remain exfoliated even in the PANI-NZM matrix. PANI-NZM contribute positively towards further exfoliation of few-layered graphite, giving higher chances of formation of single-layered graphene. Few layered graphites, including some amount of graphene, can be seen covering the PANI nanofibres. This happens due to the negative zeta value of graphene, and the positive value of PANI, wherein a layer-by-layer mechanism is being followed. PANI nanofibres act as an exfoliating agent to further exfoliate the already few-layered graphite. PANI and

graphene in this sample are taken as an equal mass, giving an overall positive surface charge.

HR-TEM

In Fig. 11, magnification at 100 nm shows a petal-like structure of sodium zinc molybdate fallen from a flower morphology, upon irradiation of electron beam (330 kV). SAED (Selective Area Electron Diffraction) patterns show an ideal lattice formation, whose interlayer distance can be calculated using information from XRD graphs. The particle was found to be electron beam sensitive as they were getting destroyed on an exposure exceeding 1 min. At a resolution of 200 nm and 50 nm, in Fig. 12, grey

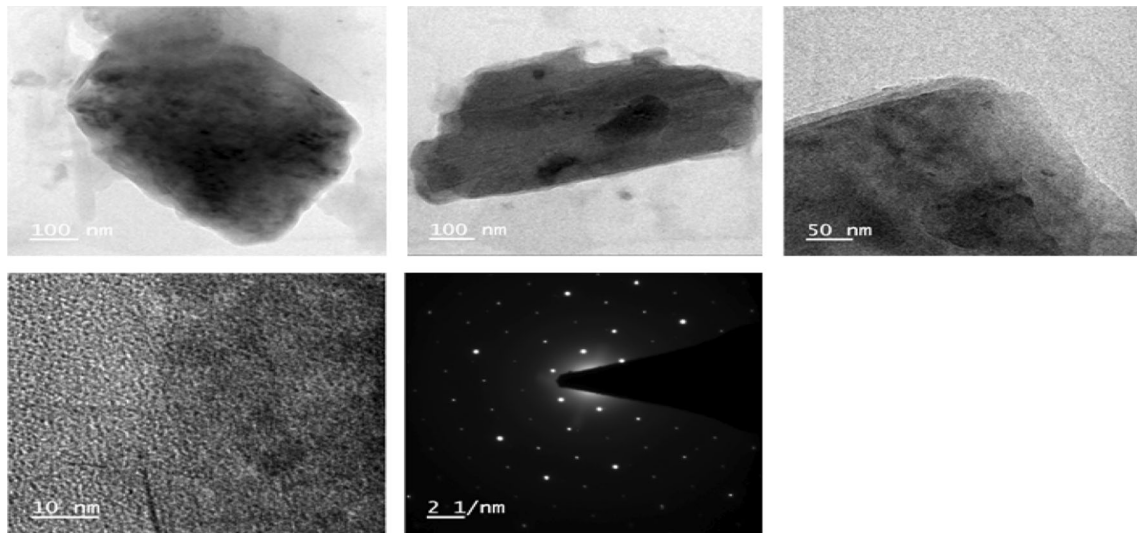


Figure 11 HR-TEM of NZM nanoparticles.

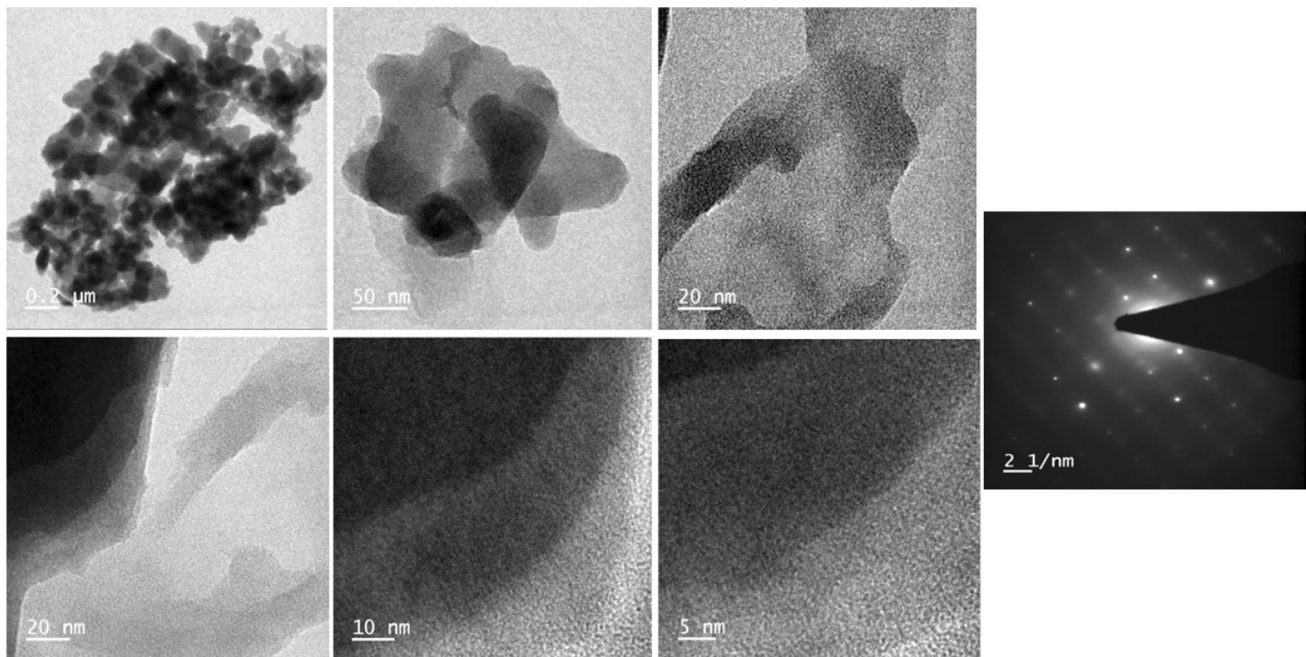


Figure 12 HR-TEM of PANI encapsulated NZM nanoparticles.

PANI encapsulation around solid black NZM particles can be seen clearly. Slight agglomeration is also seen indicated by intersecting grey portion. However, the size of NZM particles has gone below the original size due to PANI layers acting as exfoliating agents. At a resolution of 20 nm, the two layers of NZM and PANI can be differentiated clearly. At HR (High Resolution) of 10 nm and 5 nm, fringes can be observed which are very thin lines visible, parallel to each other. An appreciable observation is that the

encapsulated particles showed lower beam sensitivity than original NZM particles, and even at a very high resolution of 5 nm, the material showed distinct layers.

At a resolution of 200 nm and 100 nm, NZM-PANI nanoparticles can be seen decorated onto graphene sheets. The graphene sheets are few-layered (3–5 layers). Due to the high sheet size of graphene, it is physically very tough to wrap around small NZM-PANI particles; hence, they prefer to act as a

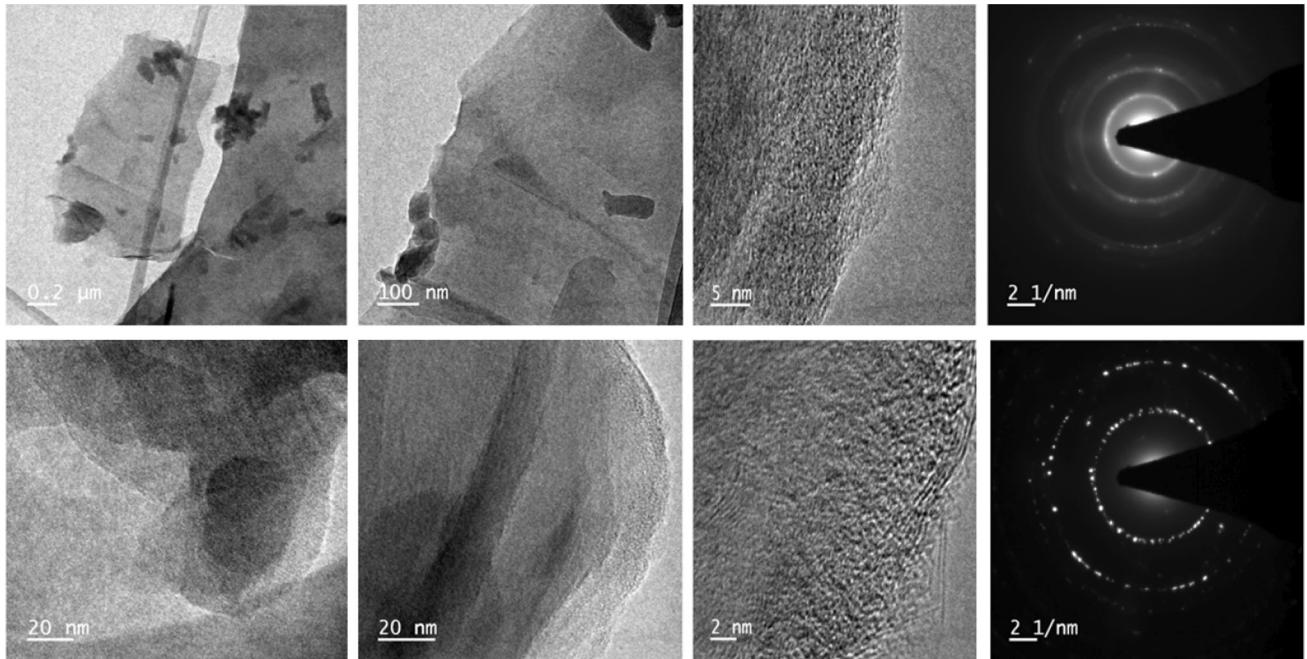


Figure 13 HR-TEM of NPG.

decorating substrate. Thus, NZM-PANI nanoparticles are sandwiched between graphene layers. At a resolution of 20 nm, different layers of NZM, PANI and graphene can be differentiated in Fig. 13. At a high resolution of 5 nm and 2 nm, along with different layers, fringes can be seen clearly, indicating the interlayer distance between each NZM-PANI-

graphene lattice, which can be verified by the SAED images shown in Fig. 13. The beam sensitivity of NZM-PANI-Graphene was the least amongst all 3 types of nanoparticles. Thus, PANI and graphene provide a shielding effect to NZM particles against 300 eV electron beam irradiation.

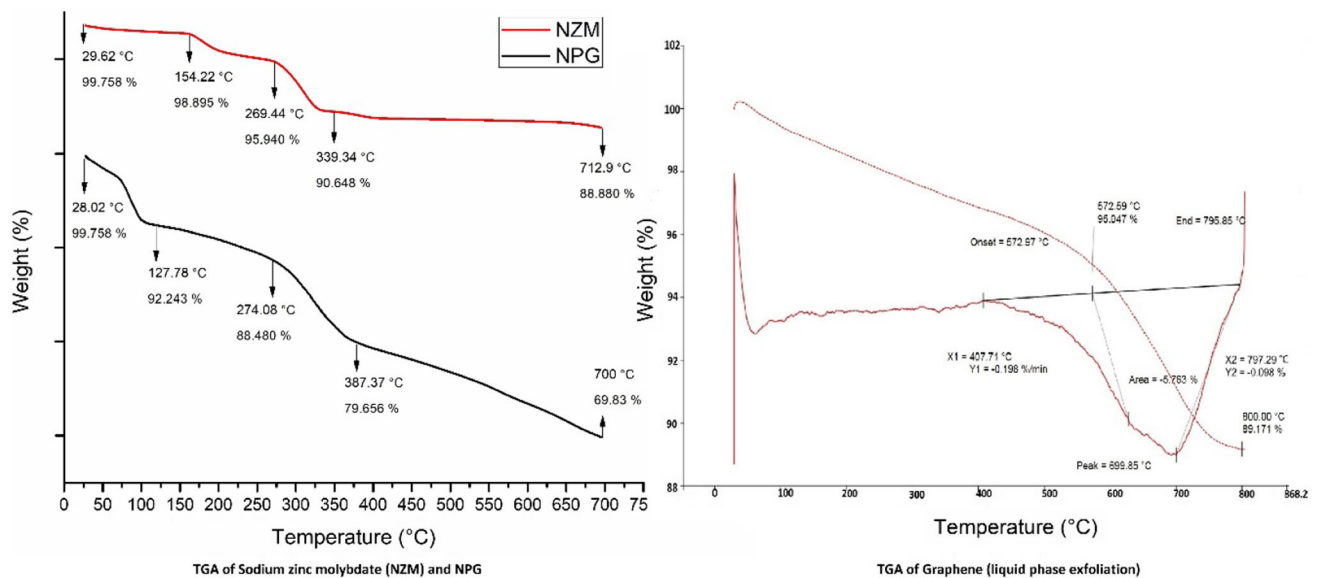


Figure 14 TGA for sodium zinc molybdate (NZM), NPG (NZM-PANI nanoparticles decorated onto graphene sheets), graphene (Liquid-phase exfoliation).

TGA

Figure 14 shows the behaviour of NZM (Sodium zinc molybdate) where there is a major decrease in weight at 154.22 °C, 269.44 °C, and 339.34 °C showing sodium, zinc and molybdenum degradation temperature. The figure shows the degradation curve for liquid-phase exfoliated graphene. Onset was seen at 572.97 °C, showing temperature stability for high temperatures. The graph shows the presence of graphite and multi-layered graphenes due to 5 wt% material loss up to onset temperature. The figure shows three onset points, indicating a 3-material system. The heat stability of the product had increased due to the incorporation of graphene. The first onset temperature was at 110 °C, followed by 127.78 °C, and 274.08 °C. The final degradation temperature was found to be 387.37 °C.

Corrosion tests

Salt spray test (SST)

Figure 15 shows the salt spray test in which all additives were taken in the ratio of 1wt% to total batch size (Epoxy + Polyetheramine). Figure A shows corrosion during a scratch test, on the neat epoxy coating. Figure B shows lesser corrosion, although there is some delamination, indicating low adherence to the substrate. However, NZM could provide adequate corrosion protection. Figure C shows PANI incorporation into the epoxy matrix and shows better corrosion protection than neat epoxy, and higher adherence than NZM, as PANI, forms a passivating layer with good adherence to the substrate. Figure D shows the incorporation of NZM-PANI-Graphene nanocontainers and shows the best performance in terms of corrosion protection, as there is no presence of rust even after 500 h of immersion (ASTM B-117).

Figure 15 A Neat Epoxy, B NZM + Epoxy, C PANI + Epoxy, D NZM-PANI-Graphene + Epoxy(500 h salt spray immersion).

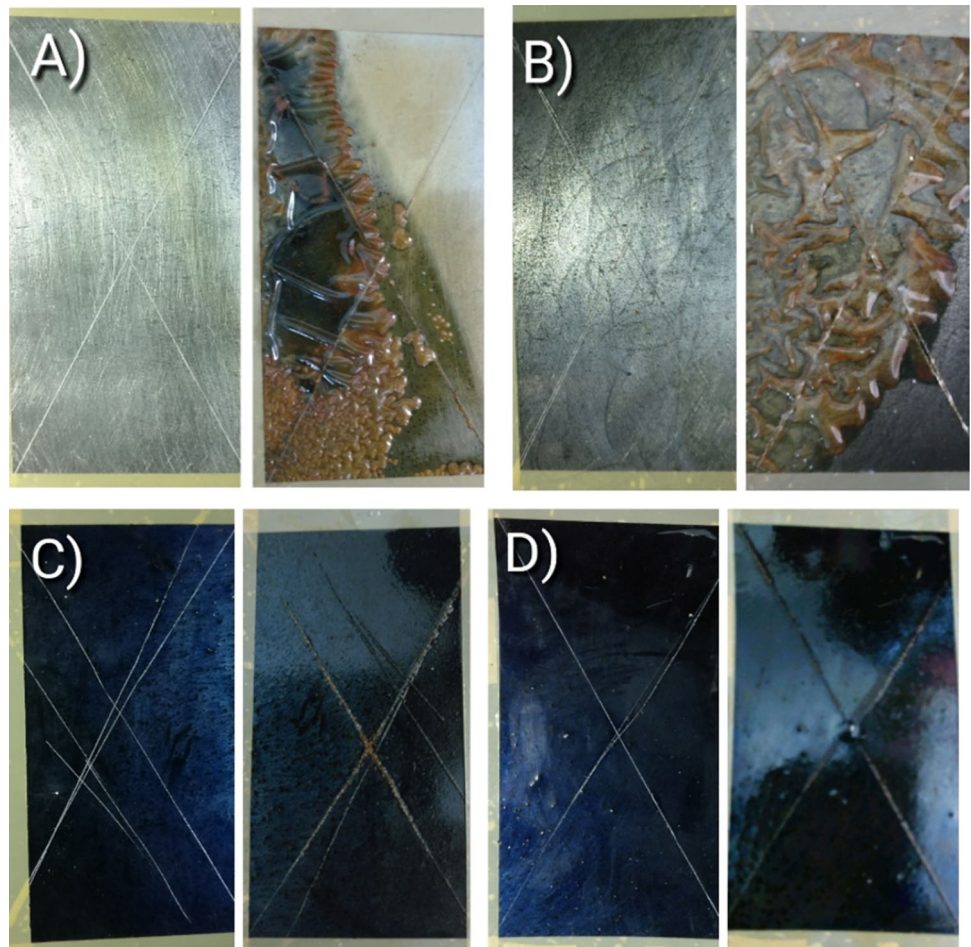
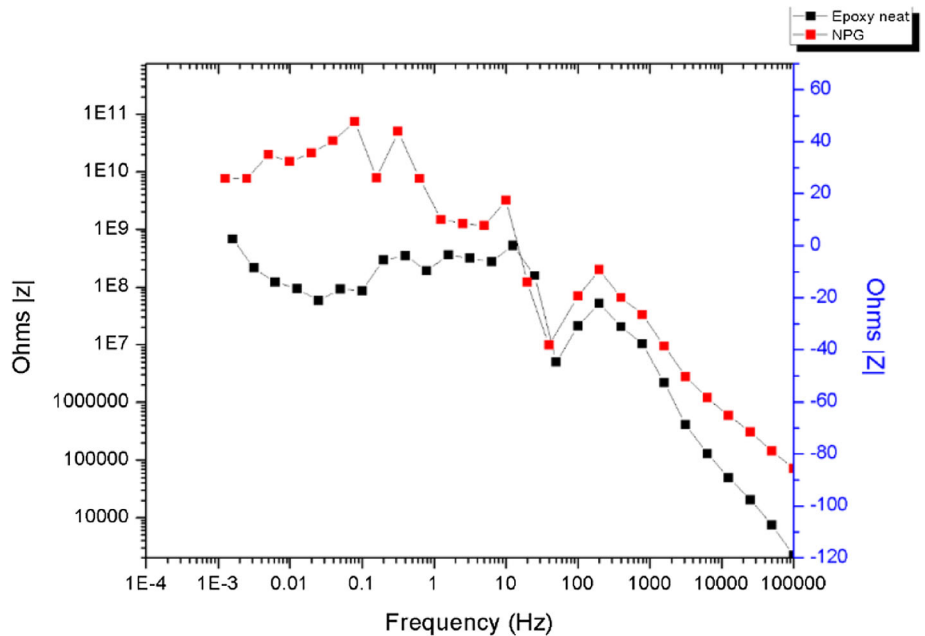


Figure 16 Bode plot (Epoxy neat vs 1wt% NPG).



Bode plot

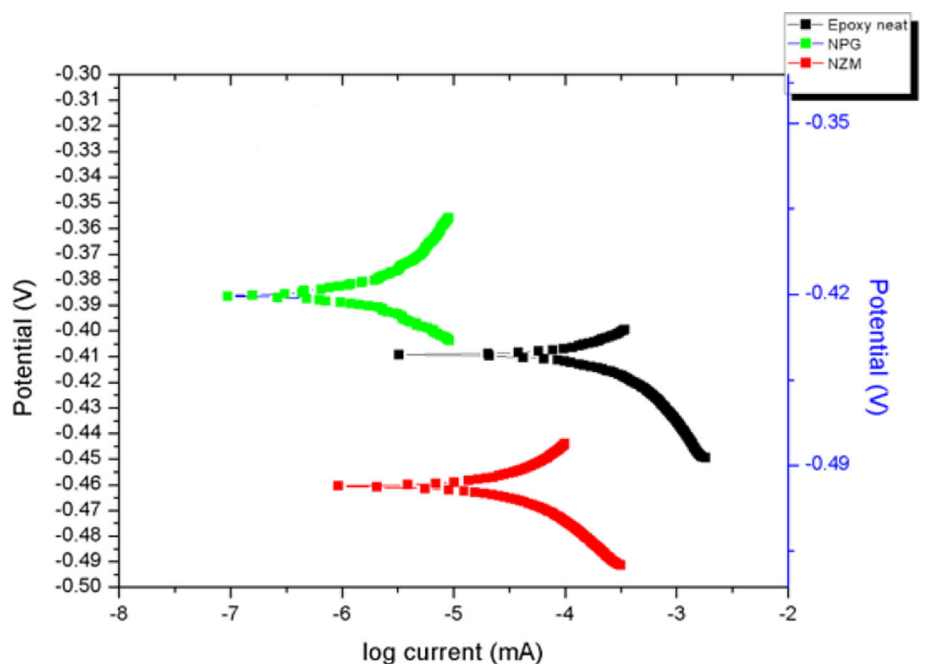
Generally, a higher Z modulus at a lower frequency indicates better corrosion resistance. It can be seen in Fig. 16 after the incorporation of 1wt% NPG, the corrosion resistance increases, and the initial z value increases 50 ×. The test was carried out after 2 h of immersion in a salt solution. The irregular drops in current value accompanied with a sudden increase seen for NPG incorporated curve indicate self-

healing effect is shown when electrolyte shell begins to deplete and core particles form a passivating layer.

Tafel plot

The measuring cell consisted of a working electrode (2 K epoxy-polyamide clear-coated and 2 K epoxy-polyamide-sodium zinc molybdate-coated low carbon steel panels), stainless steel as a counter electrode, and a saturated calomel reference electrode.

Figure 17 Tafel plot (Epoxy neat–black, NPG–green, NZM–red).

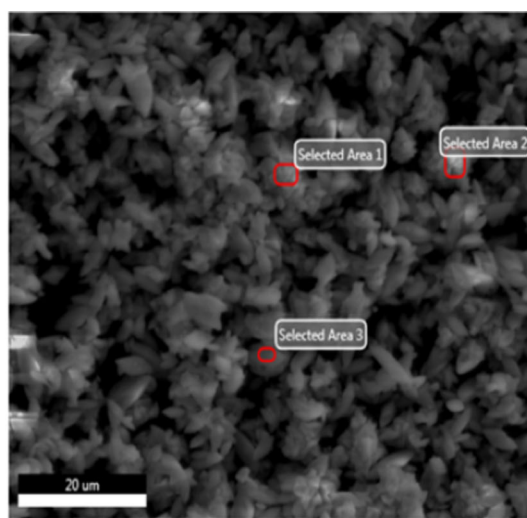


The cell was coupled with Gamry Reference system 600 (Wilmington, the USA) for corrosion studies. The corrosion protection performance of coated samples was assessed by potentiodynamic polarization. The frequency range was between 0.01 and 100 Hz, and data were recorded in terms of the Bode plot. The scan rate was 200 mV/s. In Fig. 17, Tafel plot is plotted between potential and $\log(\text{current})$ as observed with 3.5wt% NaCl solution. The test was carried out once the OCP (Open Circuit Potential) had reached. Corrosion performance can be calculated by using the slope of the Tafel plot and observing an increase/decrease in current density with respect to overpotential. Overpotential is the difference between applied potential and corrosion

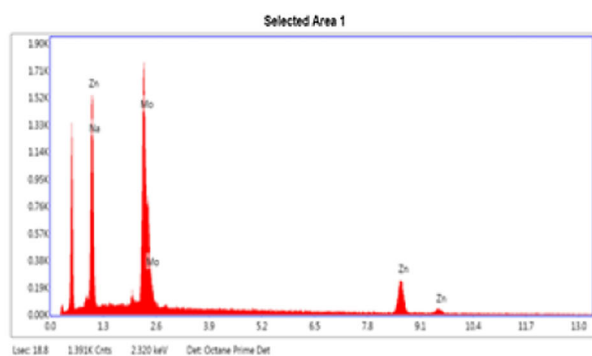
potential. It can be seen that the current density decreases in all cases where NZM, NPG are being incorporated into the neat epoxy coating. NPG shows the highest overpotential, whereas NZM shows the least. A platinum electrode was used as the counter electrode, and saturated calomel electrode was used as a reference, against which applied potential is measured. The observations were potentiodynamic, and linear polarisation was used to plot the Tafel plot.

EDAX

As shown, sodium, molybdenum and potassium are in the ideal atomic ratio (33.33% each) which is

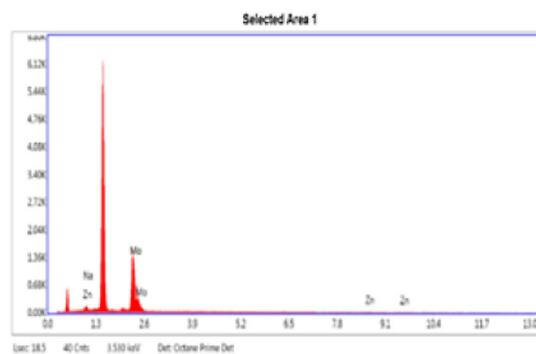


EDAX of NZM



eZAF Smart Quant Results

Element	Weight %	Atomic %	Net Int.	Error %	Kratio	Z	R	A	F
NaK	12.74	34.32	125.32	12.85	0.0388	1.2176	0.8498	0.2495	1.0023
MoL	56.40	36.42	786.18	4.10	0.4545	0.9417	1.0581	0.8475	1.0098
ZnK	30.86	29.25	190.23	5.74	0.3383	1.0243	0.9897	0.9797	1.0022



eZAF Smart Quant Results

Element	Weight %	Atomic %	Net Int.	Error %	Kratio	Z	R	A	F
NaK	0.01	0.04	0.05	99.99	0.0000	1.2888	0.8024	0.2850	1.0045
MoL	97.01	95.85	725.71	2.72	0.9856	0.9076	1.0324	0.9881	1.0098
ZnK	2.97	4.30	0.31	53.09	0.0362	1.0993	0.9558	0.9686	1.1425

Figure 18 EDAX of sodium zinc molybdate nanoparticles (novel approach).

theoretically that of sodium zinc molybdate. While that with reactivity ratio (1:1) is shown in Fig. 18. Zinc molybdate is formed predominantly, due to washing away sodium ions as water-soluble sodium nitrate.

Conclusions

The FTIR, SEM, TEM images show successful grafting of layers and hence proper encapsulation of the selected core, i.e. sodium zinc molybdate. Zeta potential and particle size characterisations show successful reversal of surface charges and particle size buildup indicating completion of the synthesis. Self-healing property is also shown due to passivating effect of core particles on the depletion of electrolyte shells which can be seen in the bode plot. EIS plots indicate high corrosion protection by nanoparticles, showing more amount of cathodic protection as E_{corr} values are more positive than neat coating. Excellent anti-corrosive performance was achieved with good dispersibility in the paint system was observed. The overall cost of the process is optimised by keeping the synthesis process as low as possible. Novel synthesis methods proved to be successful for the synthesis of NZM, PANI and NZM-PANI-Graphene.

Acknowledgements

The authors would like to acknowledge the Institute of Chemical Technology, Mumbai, for the instrumental facility.

Declarations

Conflict of interest The authors declared that there is no conflict of interest.

References

- [1] Ameen S, Seo H, Akhtar MS, Shik H (2012) Novel graphene / polyaniline nanocomposites and its photocatalytic activity toward the degradation of rose Bengal dye. *Chem Eng J* 210:220–228
- [2] Li R, Liu L, Yang F (2013) Preparation of polyaniline / reduced graphene oxide nanocomposite and its application in adsorption of aqueous Hg (II). *Chem Eng J* 229:460
- [3] De Castro RK et al (2015) New transfer method of CVD-grown graphene using a flexible transparent and conductive polyaniline-rubber thin film for organic electronic applications. *Chem Eng J* 273:509
- [4] Omaish M, Mansoob M, Ali S, Amal I, Lee J, Hwan M (2014) pTSA doped conducting graphene / polyaniline nanocomposite fibers: thermoelectric behavior and electrode analysis. *Chem Eng J* 242:155–161
- [5] Luo H et al (2017) Constructing 3D bacterial cellulose/graphene/polyaniline nanocomposites by novel layer-by-layer in situ culture toward mechanically robust and highly flexible freestanding electrodes for supercapacitors. *Chem Eng J* 334:1148
- [6] Zhao Y, Ma J, Chen K, Zhang C, Yao C (2017) One-pot preparation of graphene-based polyaniline conductive nanocomposites for anticorrosion coatings. *NANO* 12(5):1–9
- [7] Shahri Z, Bazarganipour M, Salavati-niasari M (2013) Superlattices and microstructures controllable synthesis of novel zinc molybdate rod-like nanostructures via simple surfactant-free precipitation route. *Superlattices Microstruct* 63:258–266
- [8] Lin Y, Jin J, Song M (2011) Preparation and characterisation of covalent polymer functionalized graphene oxide. *J Mater Chem*. <https://doi.org/10.1039/C0JM01859G>
- [9] Si Y, Samulski ET, Hill C, Carolina N (2008) Synthesis of Water Soluble Graphene. *Nano Lett* 8(6):1679
- [10] Jing X, Wang Y, Wu D, Qiang J (2007) Sonochemical synthesis of polyaniline nanofibers. *Ultrason Sonochem* 14:75–80
- [11] Guo Q, Yi C, Zhu L, Yang Q, Xie Y (2005) Chemical synthesis of cross-linked polyaniline by a novel solvothermal metathesis reaction of p -dichlorobenzene with sodium amide. *Polymer* 46:3185–3189
- [12] Dong X et al (2011) The formation of a carbon nanotube – graphene oxide core – shell structure and its possible applications. *Carbon* 9:1–8
- [13] Xie S et al (2014) *Electrochimica Acta* Synthesis of polyaniline-titania nanotube arrays hybrid composite via self-assembling and graft polymerization for supercapacitor application. *Electrochim Acta* 120:408–415
- [14] Kohl M, Kalendova A, Bla M, Stejskal J, Erben M (2017) Corrosion protection by organic coatings containing polyaniline salts prepared by oxidative polymerization. *J Coat Technol Res* 14(6):1397
- [15] Schniepp HC et al (2006) Functionalized single graphene sheets derived from splitting graphite oxide. *J Phys Chem B* 110(17):8535–8539

- [16] Wei T, Fan Z, Luo G, Zheng C, Xie D (2009) A rapid and efficient method to prepare exfoliated graphite by microwave irradiation. *Carbon* 47(1):337–339
- [17] Choucair M, Thordarson P, Stride JA (2009) Gram-scale production of graphene based on solvothermal synthesis and sonication. *Nat nanotechnol* 4(1):30–33
- [18] Lin B, Lu J, Kong G (2008) Effect of molybdate post-sealing on the corrosion resistance of zinc phosphate coatings on hot-dip galvanized steel. *Corros sci* 50(4):962–967
- [19] Nobrega MM, Martins VL, Torresi RM, Temperini MLA (2014) One-step synthesis, characterization and properties of emeraldine salt nano fibers containing gold nanoparticles. *J Phys Chem* 118(8):4267
- [20] Marcano DC et al (2010) Improved synthesis of graphene oxide. *ACS Nano* 4(8):4806–4814
- [21] Li Y, Xu Y, Wang S, Wang H, Li M, Dai L (2019) Preparation of graphene/polyaniline nanocomposite by in situ intercalation polymerization and their application in anti-corrosion coatings. *High Perform Polym* 31(9–10):1226–1237
- [22] Sajid S, Shah A, Nasir H (2017) Liquid-phase exfoliation of few-layer graphene and effect of sonication time on concentration of produced few layer graphene. In *Nano Hybrids Compos* 14:17–24
- [23] Kapole SA et al (2014) Investigation of corrosion inhibition performance of ultrasonically prepared sodium zinc molybdate nanopigment in two-pack epoxy-polyamide coating. *Compos Interface* 21(9):833–852
- [24] Zhao X, Meng G, Han F, Li X, Chen B, Xu Q (2013) Nanocontainers made of various materials with tunable shape and size. *Sci Report J* 3(1):1–7
- [25] Wang H, Ren H, Jing C, Li J, Zhou Q, Meng F (2020) (2021) Two birds with one stone: Graphene oxide@sulfonated polyaniline nanocomposites towards high-performance electromagnetic wave absorption and corrosion protection. *Compos Sci Technol* 204:108630
- [26] Qian B, Song Z, Hao L, Wang W, Kong D (2017) Self-healing epoxy coatings based on nanocontainers for corrosion protection of mild Steel. *J Electrochem Soc* 164(2):54–60
- [27] Shchukin BDG, Zheludkevich M, Yasakau K, Lamaka S, Ferreira MGS, Möhwald H (2007) Layer-by-layer assembled nanocontainers for self-healing corrosion protection. *Adv mater* 18(3):1672–1678
- [28] Tan CK, Blackwood DJ (2003) Corrosion protection by multilayered conducting polymer coatings. *Corros Sci* 45:545–557
- [29] Wang F, Drzal LT (2015) Mechanical properties and thermal conductivity of graphene nanoplatelet / epoxy composites. *J Mater Sci* 50(3):1082–1093. <https://doi.org/10.1007/s10853-014-8665-6>
- [30] Ramezanzadeh B, Bahlakeh G, Ramezanzadeh M (2018) Polyaniline-cerium oxide (PAni-CeO₂) coated graphene oxide for enhancement of epoxy coating corrosion protection performance on mild steel. *Corros Sci* 137:111–126
- [31] Singh HK, Yeole KV, Mhaske ST (2016) Synthesis and characterization of layer-by-layer assembled magnesium zinc molybdate nanocontainer for anticorrosive application. *Chem Eng J* 295:414–426
- [32] Jalilov AS (2016) Anticorrosion coatings based on zinc phosphate and zinc molybdate nanoparticles. *J Mole Eng Mater* 4(4):2–5
- [33] Qiang J, Yu Z, Wu H, Yun D (2008) Polyaniline nanofibers synthesized by rapid mixing polymerization. *Synth Metals* 158:544–547
- [34] Tung VC, Allen MJ, Yang Y, Kaner RB (2009) High-throughput solution processing of large-scale graphene. *Nat Nanotech* 4(2008):25–29
- [35] Adhikari A et al (2017) Corrosion resistant hydrophobic coating using modified conducting polyaniline. *High Perform Poly* 30(2):181
- [36] Yi M, Shen Z, Zhang X, Ma S (2013) Achieving concentrated graphene dispersions in water / acetone mixtures by the strategy of tailoring Hansen solubility parameters. *J Phys D J Appl Phys* 46(2):025301
- [37] Kinlen PJ, Menon V, Ding Y, Kinlen PJ, Menon V, Ding Y (1999) A mechanistic investigation of polyaniline corrosion protection using the scanning reference electrode technique a mechanistic investigation of polyaniline corrosion protection using the scanning reference electrode technique. *J Electrochem Soc* 146(10):3690–3695
- [38] Bhanvase BA, Patel MA, Sonawane SH, Pandit AB (2016) Ultrasonics Sonochemistry Intensification of ultrasound-assisted process for the preparation of spindle-shape sodium zinc molybdate nanoparticles. *Ultrason Sonochem* 28:311–318
- [39] Baker CO, Huang X, Nelson W, Kaner RB (2017) Polyaniline nanofibers: broadening applications for conducting polymers. *Chem Soc Rev* 46(5):1510–1525

Publisher's Note Springer Nature remains neutral with regard to jurisdictional claims in published maps and institutional affiliations.